Supplemental Figures 1-5

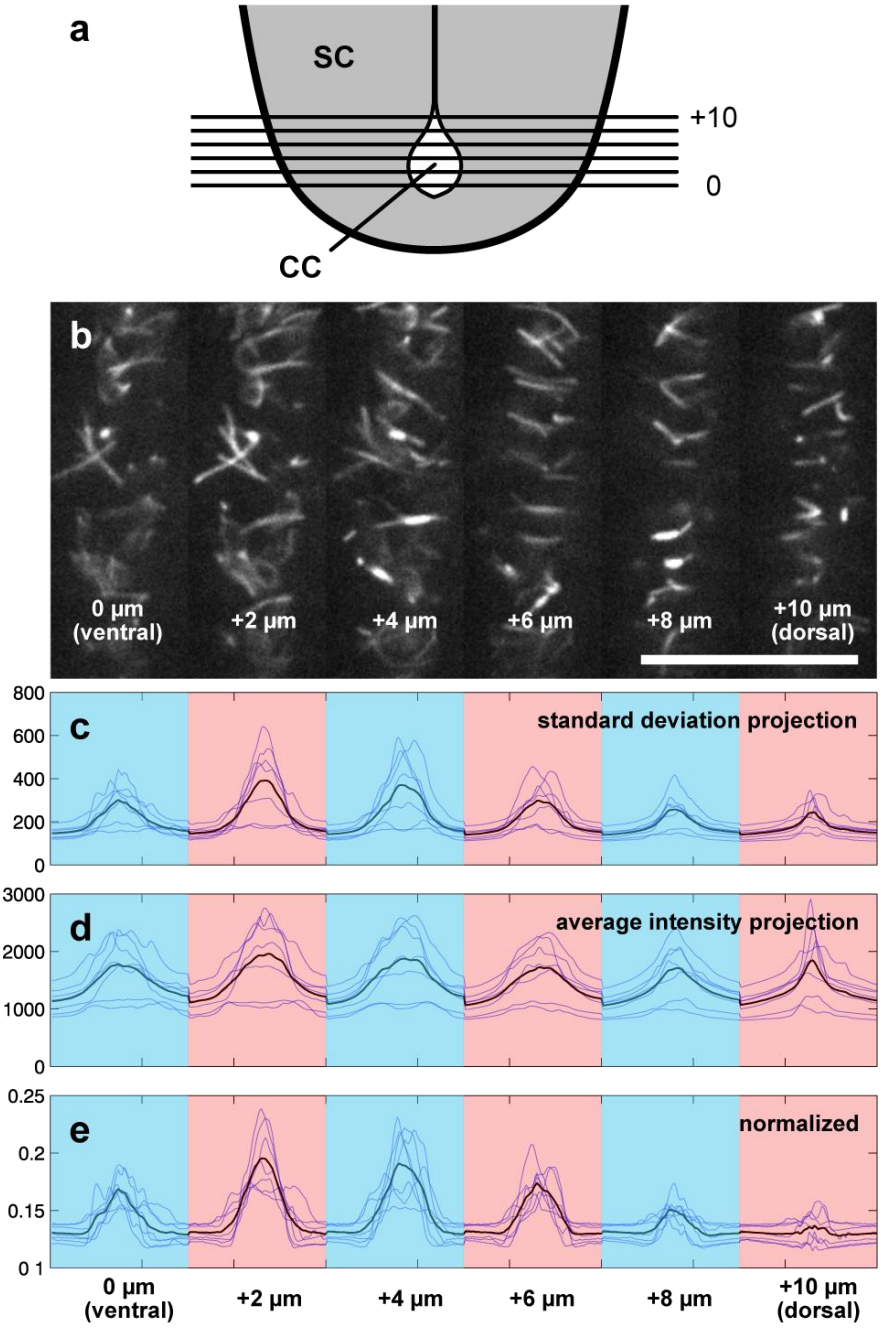

Supplementary Fig. 1. Estimation of wild type ciliary motion as a function of position in the dorsoventral axis.
(a) Schematic illustrating ciliary imaging experiments. Time-lapses are taken from optical slices covering the central canal moving ventral to dorsal 2 µm apart. (b) Representative frame from a conjoined time-lapse showing 6 planes of central canal cilia. Scale: 25 µm. (c) Intensity plot profiles derived from standard deviation projections. Blue traces are individual embryos, black trace represents average across all embryos. Blue and pink coloration defines the optical section. (d) Intensity plot profiles derived from average intensity projections. (e) Normalized profiles generated by dividing individual standard deviation profile plots by average intensity profile plots reveal a greater motility 2 - 4 µm away from the ventral boarder of the central canal.

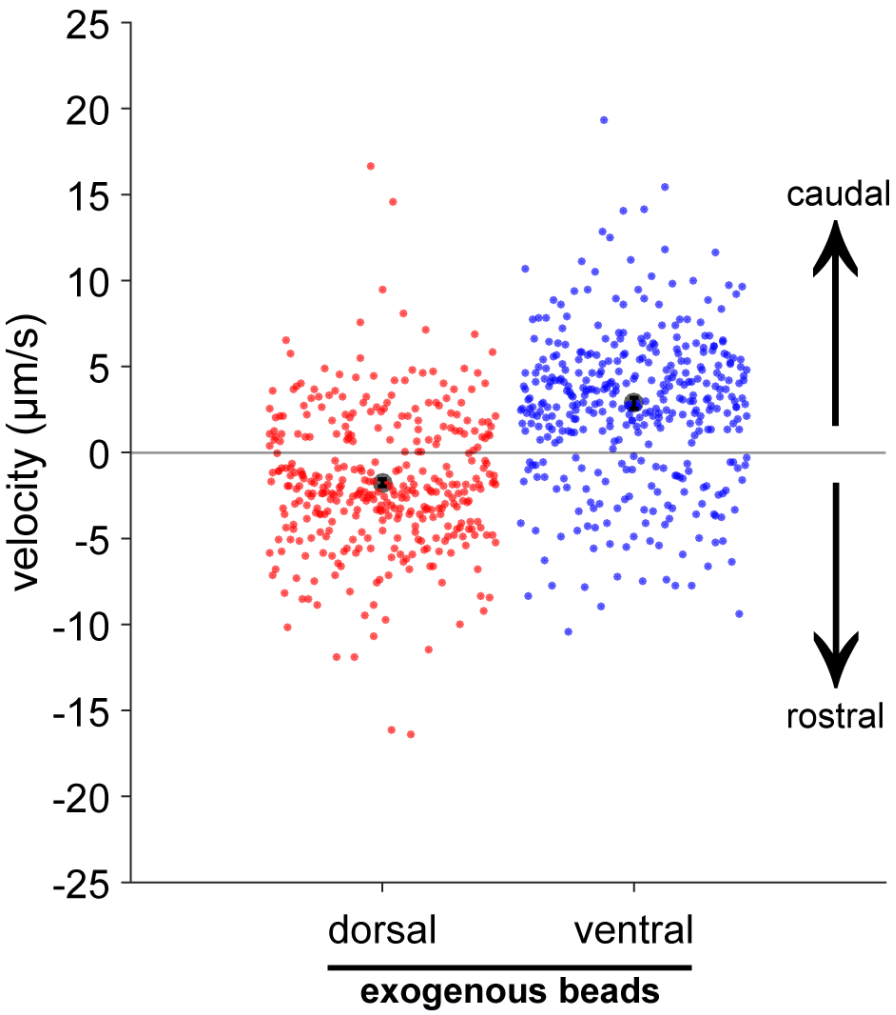

Supplementary Fig. 2. Bidirectional flow of the CSF in the central canal is preserved in the *pkd2l1*$^{-/-}$ mutant.
Each point represents one tracked trajectory. Error bars indicated standard error of the mean. Net dorsal movement is posterior to anterior; net ventral movement is from anterior to posterior. Dorsal mean velocity: 1.76 +/- 0.21 µm/s; ventral mean velocity: 2.86 µm/s +/- 0.32 µm/s. n = 362 dorsal trajectories, n = 381 ventral trajectories from n = 5 *pkd2l1*$^{-/-}$ embryos.

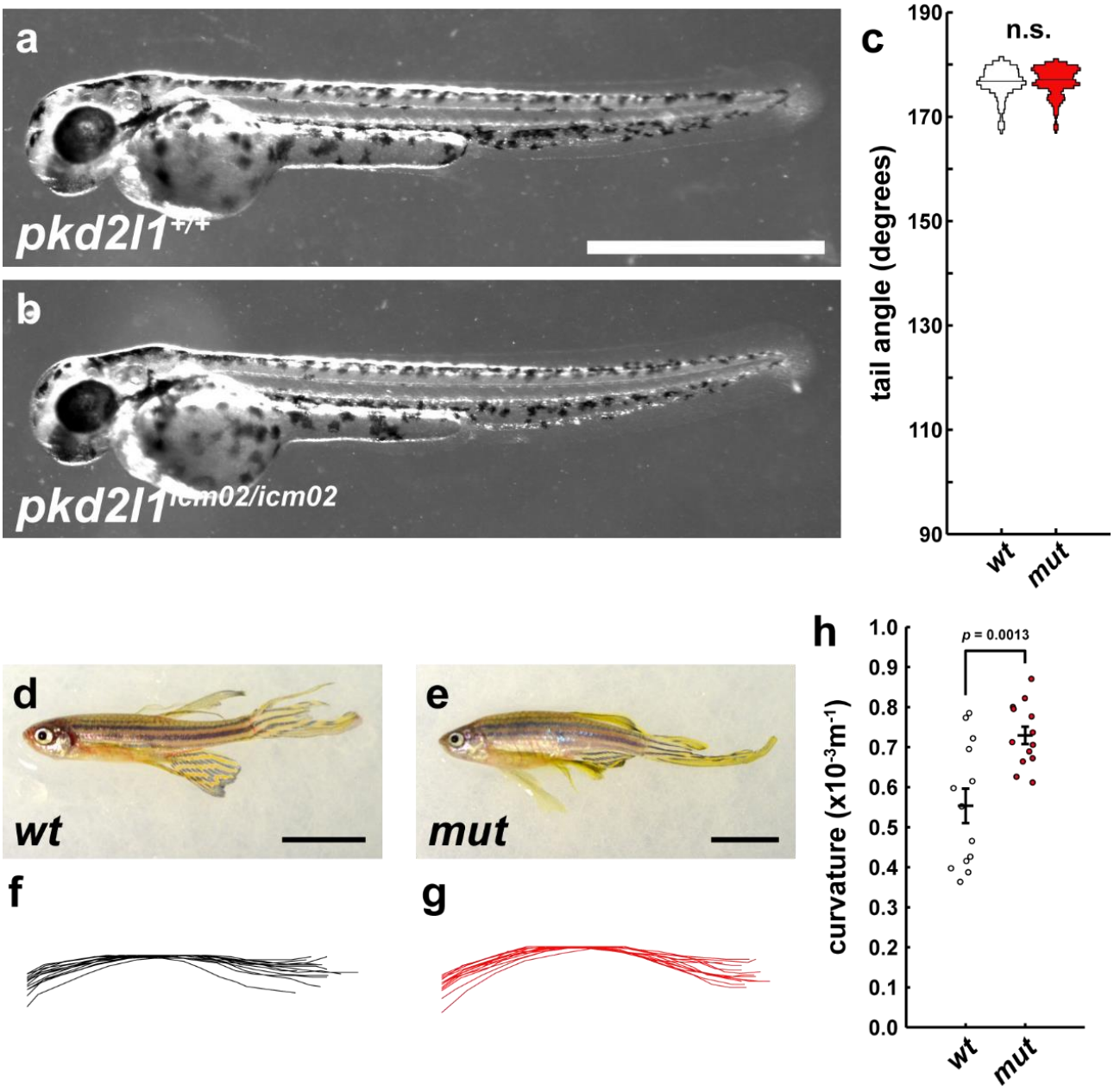

Supplementary Fig. 3. After three generations, *pkd2l1*$^{icm02/icm02}$ fish continue to develop kyphosis as adults.
(a) 48 hpf wild-type larva exhibiting normal development and a near 180° tail angle. Scale bar: 1 mm. (b) No difference is observed in the 48 hpf *pkd2l1*$^{icm02/icm02}$ larvae. (c) Violin plot of tail angles comparing a wild-type clutch to a mutant clutch at 48 hpf; there is no significant difference in tail angle. (d) Wild-type adult fish at 12 months. Scale bar: 1 cm. (e) *pkd2l1*$^{icm02/icm02}$ adult fish at same age. Scale bar: 1 cm. (f) Traces of spinal curvature derived from widefield images taken of wild-type adults. (g) Same traces from *pkd2l1*$^{icm02/icm02}$ mutant adults. (h) Quantitative comparison of spinal curvature between wild-type and mutant adults at 12 months. Mutant spinal curvature is significantly greater.

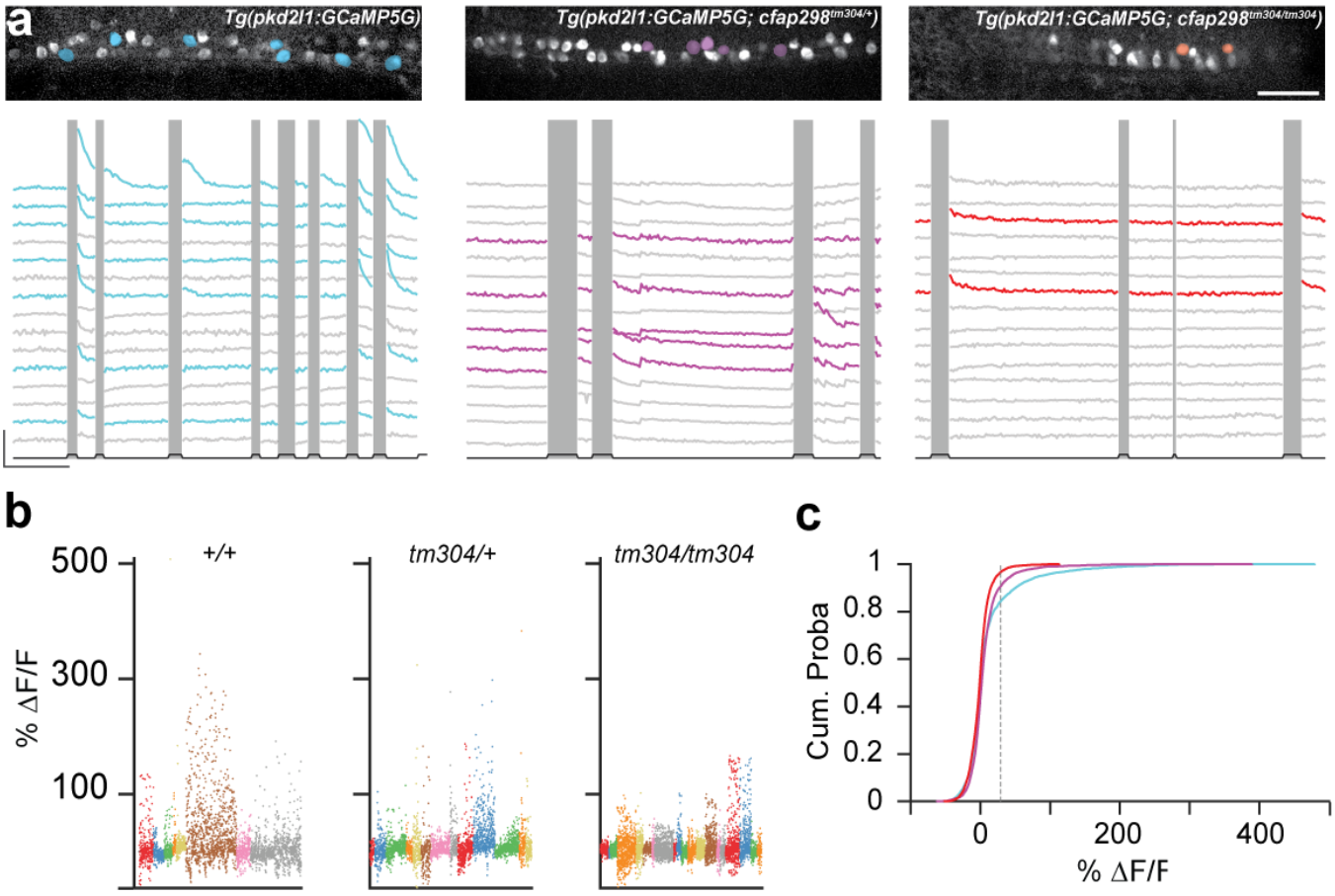

Supplementary Fig. 4. The *cfap298* mutation does not abolish sensory responses to muscle contraction in 1 dpf zebrafish.
(a) Top: Images of *Tg(pkd2l1:GCaMP5G)* in *cfap298*$^{+/+}$, *cfap298*$^{tm304/+}$, *cfap298*$^{tm304/tm304}$. Scale: 50 µm. Bottom: Sample calcium imaging traces of CSF-cNs at 1 dpf during active muscle contractions. Gray bars indicate periods of contraction when the cell moves out of the imaging plane. Scale: 10 s, 100% ΔF/F. (b) Responses to muscle contractions in individual cells for each genotype (*cfap298*$^{+/+}$ n = 7 fish, 140 cells; *cfap298*$^{tm304/+}$ n = 12 fish, 275 cells; *cfap298*$^{tm304/tm304}$ n = 20 fish, 430 cells). (c) Cumulative distribution plot of the responses for all genotypes shows a reduced response of CSF-cNs to spontaneous contraction in *cfap298*$^{tm304/tm304}$ embryos (p = 0.0005, repeated measures ANOVA using a linear mixed model).

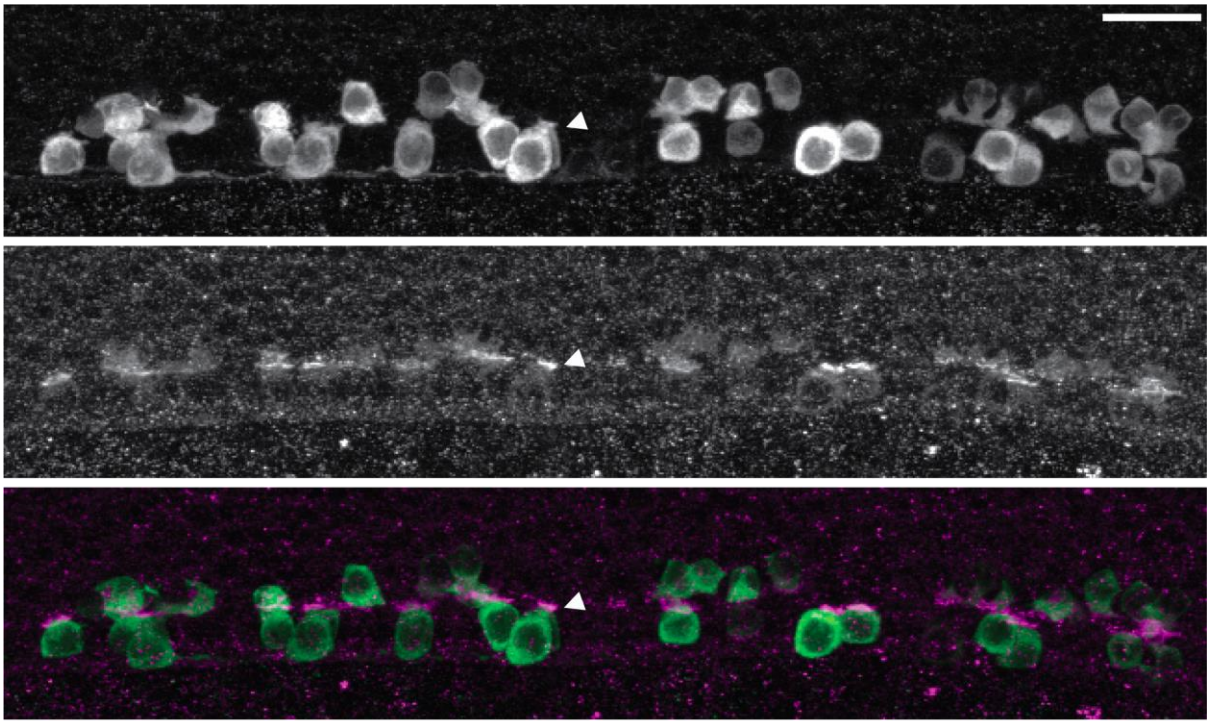

Supplementary Fig. 5. Pkd2l1 is correctly localized to the apical extension in the *cfap298*$^{m304/tm304}$ mutant.
Pkd2l1 immunohistochemistry in *Tg(pkd2l1:GCaMP5G; cfap29*$^{tm304/tm304}$*)* at 30 hpf. Top: GFP staining, middle: Pkd2l1 staining, bottom: merge, GFP staining is in green, Pkd2l1 staining is in magenta. Scale: 20 µm.

Supplementary Table 1. Statistics for Figure 1a-b

		Imaging plane 1					
		0 µm	2 µm	4 µm	6 µm	8 µm	10 µm
Imaging plane 2							
	2 µm	0.0303					
	4 µm	0.0498	0.9999				
	6 µm	0.9976	0.0857	0.1323			
	8 µm	0.4127	0.0001	0.0003	0.1996		
	10 µm	0.079000	0.0	0.0	0.0277	0.9444	

Supplementary Table 2. Cobb angles for adult zebrafish

fish	ant. angle (°)	post. angle (°)	Cobb angle (°)
wild type 1	87.6	90	2.4
wild type 2	88.7	93.6	4.9
wild type 3	93.4	90.9	2.5
pkd2l1$^{-/-}$ 1	100.7	83	17.7
pkd2l1$^{-/-}$ 2	95.8	86.4	9.4
pkd2l1$^{-/-}$ 3	76.6	99.5	22.9

Supplementary Table 3. Zebrafish transgenic lines used in this study

Name used	Alternate name	Labeling	Original publication
pkd2l1^{icm02}	N/A	N/A	Böhm et al., 2016[20]
cfap298^{tm304}	*kurly*^{tm304} *; c21orf59* ^{tm304}	N/A	Brand et al., 1996[10]
Tg(pkd2l1:GCaMP5G)	*Tg(pkd2l1:GCaMP5G)*^{icm07}	CSF-cNs	Böhm et al., 2016[20]
Tg(pkd2l1:gal4)	*Tg(pkd2l1:gal4)*^{icm10}	CSF-cNs	Fidelin et al., 2015[39]
Tg(UAS:TagRFP-CAAX)	*Tg(UAS:tagRFP-CAAX;cmcl2:eGFP)*^{icm22}	N/A	Böhm et al., 2016[20]
Tg(UAS:mCherry)	N/A	N/A	Herwig Baier Lab
Tg(β-actin:Arl13-GFP)	*Tg(actb2:Mmu.Arl13b-GFP)*	cilia	Borovina et al., 2010[15]
Tg(olig2:DsRed2)	N/A	olig2+ cells	Kucenas et al., 2008[45]

Legends for Supplementary movies 1-6

Movie S1. Cilia in a 24 hpf *Tg(β-actin:Arl13-GFP)* embryo. Images were acquired at 33 Hz and are played in real time.

Movie S2. Imaging of exogenous beads in the central canal of the spinal cord in a wild type embryo. Images were acquired at 10 Hz and are played in real time.

Movie S3. Imaging of endogenous particles with FF-OCT in the central canal of the spinal cord in a 26-28 hpf *Tg(β-actin:Arl13-GFP)* embryo. Images were acquired at 100 Hz and are played in real time.

Movie S4. Calcium imaging of CSF-cNs in a wild type *Tg(pkd2l1:GCaMP5G)* embryo at 24-26 hpf. Images were acquired at 4 Hz and are sped up 5x in the movie.

Movie S5. Calcium imaging in CSF-cNs in a *cfap298*$^{m304/tm304}$ *Tg(pkd2l1:GCaMP5G)* embryos at 24-26 hpf. Images were acquired at 4 Hz and are sped up 5x in the movie.

Movie S6. Calcium imaging of CSF-cNs in a *pkdl21*$^{-/-}$ *Tg(pkd2l1:GCaMP5G)* embryo at 24-26 hpf. Images were acquired at 4 Hz and are sped up 5x in the movie.